Investigation of Mechanical, Thermal, Electrical, and Hydrogen Diffusion Properties in Ternary V–Ti–X Alloys: A Density Functional Theory Study

H. Alipour, M. Asgari Bajgirani, Mehdi Sahihi

Investigation of mechanical, thermal, electrical, and hydrogen diffusion properties in ternary V-Ti-X alloys: a density functional theory study

H. Alipour[a], M. Asgari Bajgirani[b], M. Sahihi[c,*]

[a] *Department of Energy Engineering, Shahid Beheshti University, Tehran, Iran*

[b] *Department of Physical Chemistry, Faculty of Chemistry, University of Lorestan, Lorestan, Iran*

[c] *Roberval Laboratory, Université de Technologie de Compiègne, Alliance Sorbonne Université, Compiègne 60200, France*

[*] *Corresponding author*

Mehdi Sahihi

email: sahihime@utc.fr and msahihi@icmab.es

Tel.: +34635816177

Abstract

The effects of alloying and hydrogen dissolution on the mechanical, thermal, and electrical properties of vanadium-based ternary alloys were investigated using Density Functional Theory. Our study showed that pure V has a lower solution energy than V-Ti-X alloys. Also, tetrahedral interstitial sites are more favorable than octahedral sites to be occupied by the H atoms. Furthermore, the alloys with 8 H atoms have a lower capacity than pure V system for H trapping at interstitial sites. These findings suggest that H dissolution in alloys is less probable than in pure V and the alloys are more resistant to hydrogen embrittlement, crack propagation, and fracture initiation. Indeed, V-Ti-Al shows a reliable performance and could be a viable non-Pd alloy for hydrogen separation. Studying the mechanical properties of pure V and the ternary alloys revealed that V-Ti-Ni provides the highest durability and better resistance to both external and hydrogen dissolution-induced internal stresses. The V-Ti-Pd alloy has the higher diffusion barrier energy (E_b=0.1807 eV) than pure V (E_b=0.1646 eV), indicating that the H atom faces more hindrance when diffuses across the alloy. Nonetheless, in the hydrogen separation temperature range, the V-Ti-Pd alloy has the largest thermal expansion coefficient (α=2.04810^{-5} K^{-1}) that indicates its poor thermal characteristics.

Keywords:

Hydrogen dissolution, Hydrogen embrittlement, Mechanical properties, Density Functional Theory

1. Introduction

Nowadays, the increase of environmental pollution by harmful gases has led to use hydrogen as a safe, green, and environmentally efficient energy source and a key element in energy transition [1–3]. Different methods for hydrogen storage, separation, and purification processes, such as pressure swing adsorption, cryogenic separation, and membrane separation have been developed to meet the industrial demand for high-purity H_2 [4]. Excessive hydrogen absorption and solvation happen in lattice expansion and hydrogen embrittlement (HE), and have a negative impact on the membrane's mechanical stability in hydrogen-metal applications [5,6]. In addition, hydrogen–hydrogen repulsive interactions within the membrane may cause phase transition of the structure [7]. Although Pd-based metals are mostly used in traditional hydrogen separation processes due to the high hydrogen permeability, their high cost of implementation limits their industrial scale applications [6,8–10]. Two strategies have been proposed to diminish the cost, i.e., (a) minimizing the required amount of palladium to achieve a higher dense layer [11,12], and (b) increasing the durability and life-span of these membranes which can be degraded due to poisoning and cracking by thermal cycling and mechanical stress [13,14]. Using non-Pd metal based (e.g., V, Nb and Ta) membranes is a suitable alternative because of their better hydrogen diffusivity, higher mechanical strength, and lower price [15,16]. On the other hand, the larger hydrogen permeability of group 5 metals than Pd metals, causes more HE and durability difficulties in non-Pd membranes for large-scale applications [17]. HE is the major reason for subcritical crack growth in materials, fracture initiation, and catastrophic failure with subsequent loss in mechanical properties such as ductility, toughness and strength [18]. However, alloying with different materials can alleviate this drawback. In this regard, different binary, ternary and even quaternary alloys have been provided as a new generation of materials [19,20].

Several researches have been conducted to study the performance of vanadium (V)-based binary alloys (e.g., V-Pd, V-Al, and V-Ni) and ternary alloys (e.g., V-Ni-Al, V-Ni-Fe, V-Ni-Si, V-Ni-Ti, and V-Ni-Zn) [21–24]. Tailoring the composition and (thermo-)dynamics of disordered alloys has been done with the aim of controlling hydrogen permeability in membranes, hydrogen storage capacity, kinetics of hydrogen release, and protecting materials against HE [25–27] . Although ordered and disordered (alloy) metal-hydrogen systems have been experimentally and theoretically studied, a theoretical description of metal hydrides is still helpful to provide a quantitative description for different characteristics of these materials [3,28–32].

Yanli Lu *et al.* investigated the dissolution and diffusion behaviors of hydrogen in V-based binary alloys, V-M (M=Al, Ti, Cr, Fe, Ni and Nb), using density functional theory (DFT) method. Their results revealed that H solution energies are the lowest in V-Ti alloy and using smaller size metals in the alloy increases the H solution energy and leads to the lower HE [33]. They also studied the mechanical and thermal properties of V-Ni-M alloys (M= Al, Fe, Si, Ti, Zn) and their hydrogen solubility and diffusion behaviors by first principles calculations. Their mechanical analysis indicated the best resistance to deformation for the V-Ni-Ti, the best ductility for pure vanadium,

and the smallest thermal expansion coefficient for V-Ni-Si alloy in the related application temperature range [17].

As reported in the literature, V, like the other members of group 5 transition metals (TM) (e.g., Nb and Ta), provide a good alternative for Pd-based metal membranes [15,16]. The performance of many of the V-based alloys has been studied by researchers and, V-Al [22], V-Ni[23], and V-Pd [20,21] binary alloys are among the highest attractive ones. Moreover, Ti metal has been utilized for alloying because of its good adsorption quality, as well as its superior mechanical properties and corrosion resistance [34]. J. Hua et al. calculated the interactions between H and the vacancy and defect solution energies, as well as the contributions of Ti to stability, in a dilute V–Ti binary alloy, as a candidate structural material in fusion reactors. They found that doping Ti into dilute V–Ti binary alloys inhibits the H solution and thereby suppresses hydrogen retention [35]. Kai Ma et al. examined the adsorption properties and mechanism of hydrogen molecules on Ti-decorated carbon-based hydrogen adsorbent structures using DFT calculations. According to the findings, Ti-decorated graphene appears to be a good material for hydrogen storage [36]. Also, the mechanical and structural characteristics of Ti and Ti-based alloys throughout the hydrogen absorption–desorption process at various temperatures and hydrogen concentrations have been investigated using Vickers microhardness tests and X-ray diffraction (XRD) analyses [28].

In the present study we use first-principles calculations to investigate the feasibility of forming and also the performance of the V-Ti-X (X= Al, Ni, and Pd) ternary alloys using DFT calculations. The aim is to find an alloy with the optimum behavior in respect with the HE related mechanical properties and H diffusivity. Furthermore, the mechanical, electrical and thermal properties are taken into consideration for the alloys and the H-alloys systems. It is expected that the results of this study can be used as a theoretical basis for the experimental investigations.

2. Computational Methods

All calculations related to dissolution and diffusion properties of hydrogen in V-Ti-X alloys (X=Al, Pd, Ni), and their mechanical properties were carried out by the spin-polarized DFT method using the DMol^3 module [37] implemented in Materials Studio software package. The generalized gradient approximation (GGA) method with Perdew-Burke-Ernzerhof (PBE) [38] as the exchange–correlation functional, as well as the double numerical plus polarization (DNP) basis set [39] were utilized in all the calculations. All electrons option was considered for the relativistic effect to treat the core electrons. For dispersive intermolecular interactions and long-range Van der Walls forces and DFT-D2 method proposed by Grimme scheme was used [40–42]. The three-dimensional periodic boundary condition was applied for a 2×2×2 supercell, as a symmetric model of pure V and V-based alloys (Fig. *1*). This sample contains 16 V atoms for pure V and two of which were replaced with the Ni and X atoms (X=Al, Pd, Ni) for the alloys. For integration in the first Brillouin zone, a 4×4×4 Monkhorst-Pack mesh of k-point sampling was used. The values of

10^{-5} Ha, 2×10^{-3} Ha/Å, 5×10^{-3} Å and 5.0 Å were applied as energy tolerance accuracy, maximum force, displacement and global orbital cut-off radius, respectively. The minimum energy pathway for diffusion of the H atoms was investigated by linear synchronous transit/quadratic synchronous transit (LST/QST) [43]. The Nudged Elastic Band (NEB) method [44], implemented in the DMol^3 module, was used to determine the structure of the transition state and the minimum energy reaction pathway.

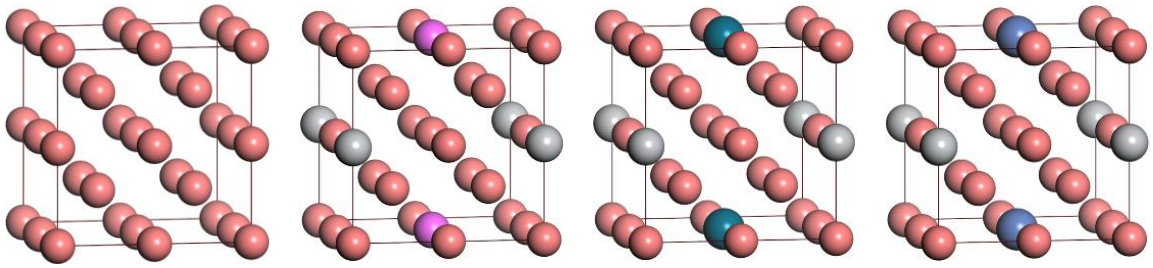

Fig. 1 Structure of (a) pure V, (b) V-Ti-Al, (c) V-Ti-Ni, and (d) V-Ti-Pd alloys. Red, gray, pink, dark green, and dark blue spheres represent V, Ti, Al, Ni, and Pd atoms, respectively.

3. Results and Discussion

3.1. Structural stability

Structural stability is one of the features that must be taken into account to characterize the feasibility of alloying of materials (in this case, pure V) with different elements. Hence, two criteria, including formation enthalpy (ΔH) and cohesive energy (E_{coh}) have been proposed as Eq. (1) and Eq. (2), respectively [45]:

$$\Delta H = \frac{1}{N_{total}}\left(E_{total} - N_V E_{bulk}^V - N_{Ti} E_{bulk}^{Ti} - N_X E_{bulk}^X\right) \quad (1)$$

$$E_{coh} = \frac{1}{N_{total}}\left(E_{total} - N_V E_{iso}^V - N_{Ti} E_{iso}^{Ti} - N_X E_{iso}^X\right) \quad (2)$$

where E_{total} and N_{total} are the total energy and total number of atoms in the cell of pure V and the alloys. N_V, N_{Ti} and N_X are the numbers of V, Ti and X (X= Al, Ni, Pd) in the samples, respectively. E_{iso} and E_{bulk} are the energy of atoms in isolated and bulk states, respectively. The calculated values of lattice constant (a), formation enthalpy (ΔH), and cohesive energy for pure V and V-Ti-X alloys are presented in Table 1.

Table 1. Calculated enthalpy of formation (ΔH), cohesive energy (E_{coh}), and lattice constant (a) of pure V and V-Ti-X alloys.

	a/Å	E_{coh}/eV	ΔH/eV
Pure V	3.0006	-5.9549	--0.0026
V-Ti-Al	3.0249	-5.8639	-0.0446
V-Ti-Ni	3.0004	-5.9507	-0.0371
V-Ti-Pd	3.0253	-5.8212	-0.0331

The negative values of cohesive energy and formation enthalpy indicate the stability of the structures. Moreover, the lower values demonstrate the higher structural stability and the better alloying ability [17]. Table 1 clearly shows that cohesive energies and formation enthalpies of V-Ti-X ternary alloys have negative values indicating their stability. Therefore, V can be alloyed with Ti, Al, Ni, and Pd. It is worth noting that pure V has a lower E_{coh} value than the V-based alloys, implying that pure V is more stable than the alloys and V-Ti-Ni has the most stable structure among the studied ternary alloys.

3. 2. Mechanical properties

Elastic constants (C_{ij}) play a critical role in understanding the mechanical stability of the materials and reflect the bond strength between the atoms and their response to the external forces [46]. They provide information about the structural, thermo-mechanical, and chemical properties of materials [47]. For a cubic system, the value of these constants is expressed by three independent elastic constants (C_{11}, C_{12} and C_{44}) according to the stress-strain approach [48]. The resistance of a material to length change caused by axial stress applied in the direction <100> on the plane (100) is denoted by $C_{11,}$ the resistance of the material to deformation generated by longitudinal stress in the direction <010> on the plane (100) is denoted by C_{12} and the resistance of the material to deformation generated by tangential shear stress on the plane (010) in the direction <001> is given by C_{44} [49,50]. Table 2 represents the calculated elastic constants of pure V and V-Ti-X alloys.

Table 2. Elastic constants (C_{ij}) of pure V and V-Ti-X alloys.

	C_{11}/GPa	C_{12}/GPa	C_{44}/GPa
Pure V	271.046	109.222	29.396
	230.98 [a]	120.17 [a]	[a] 43.77
	281.72 [b]	124.63 [b]	36.09 [b]
V-Ti-Al	233.039	105.477	33.027
V-Ti-Ni	276.305	123.178	41.822
V-Ti-Pd	240.788	97.765	31.262

[a] Experimental [51] [b] Other theoretical studies [52]

Table 2 shows that the Born rule (C_{11} >0, C_{44} >0, C_{11} >|C_{12}|, and (C_{11}+2C_{12})>0 as criteria for the mechanical stability for cubic symmetry [53]) is satisfied for pure V and V-Ti-X alloys, indicating they are mechanically stable. The mechanical properties, including the bulk modulus (B), and shear modulus (G) can be calculated from the Voigt–Reuss–Hill's approximation (VRH) based on the elastic constants C_{ij} using Eq. (3) and Eq.(4), respectively [48]:

$$B=\frac{C_{11}+2C_{12}}{3} \quad (3)$$

$$G=\frac{G_V+G_R}{2}, G_V=\frac{C_{11}-C_{12}+3C_{44}}{5}, G_R=\frac{5C_{44}(C_{11}-C_{12})}{4C_{44}+(C_{11}-C_{12})} \quad (4)$$

where V and R are the calculated values from Voigt's and Reuss's approximations, respectively. The Young's modulus (*E*) and Poisson's ratio (υ) can be obtained from the Eq.5) and Eq.(6), respectively [48]:

$$E=\frac{9BG}{3B+G} \quad (5)$$

$$\upsilon=\frac{3B-2G}{2(3B+G)} \quad (6)$$

The brittleness and ductility of the materials can also be described with different measures obtained from elastic constants, including Poisson's ratio, Pugh's ratio, and Cauchy pressure [54]. Pugh's ratio, defined as the ratio of the bulk and shear moduli (*B/G*) and considered as a criterion for the resistance of a material to the elastic and plastic deformations. The critical value of 1.75 for the Pugh's ratio is considered as the boundary between brittleness and ductility regions [55]. Cauchy pressure criterion (P_{cauchy} = (C_{12}-C_{44})/2), defining the type and angular property of atomic bonds in metals, has the critical value of zero. Its negative or positive values indicate the brittleness or ductility of materials, respectively [53,55,56]. The Poisson's ratio is defined as the induced length variations in the perpendicular direction to the loading direction [48]. Frantsevich et al., proposed that the less or greater value than 0.26 of Poisson's ratio, indicates that the material is brittle or ductile, respectively [57].

The hardness of the material as an index for its resistance to plastic deformation and the microscopic insight of the hardness is expressed as a function of the bulk and shear moduli [53]. The Vickers hardness for different crystalline materials and complex alloys is defined by Eq.(7) [58]:

$$H_V=0.92\left(\frac{G}{B}\right)^{1.137}G^{0.708} \quad (7)$$

Table 3 represents the calculated values of bulk modulus (*B*), shear modulus (*G*), Young's modulus (*E*), Lame's coefficient (λ), Poisson's ratio (υ), Cauchy pressure (P_{Cauchy}), Pugh's ratio (*B*/*G*), and Hardness (*H*) for pure V and V-Ti-X alloys.

Table 3. Calculated values of bulk modulus (*B*), shear modulus (*G*), Young's modulus (*E*), Lame's coefficient (λ), Poisson ratio (υ), Cauchy pressure (P_{Cauchy}), Pugh's ratio (*B*/*G*), and Hardness (*H*) for pure V and V-Ti-X alloys.

	B/GPa	*E*/GPa	*G*/GPa	λ/GPa	υ	*B*/*G*	P_{Cauchy}/GPa	*H*/GPa
Pure V	163.164	122.934	44.722	133.349	0.374	3.648	39.913	3.113
V-Ti-Al	147.997	117.910	43.120	119.250	0.367	3.432	36.225	3.252

V-Ti-Ni	174.221	146.572	53.407	135.566	0.358	3.262	38.678	4.009
V-Ti-Pd	145.439	119.545	43.853	116.203	0.363	3.316	33.252	3.422

From the definition of Young's modulus, as a stress-to-strain ratio, it could be inferred that it measures the tolerability of the system to resist external stress without geometrical change and known as stiffness of materials [53]. As shown in *Table 3*, alloying the pure V with Ti and Ni atoms makes the metal stiffer, while using Ti-Al and/or Ti-Pd decreas the tolerability of the alloy to withstand external stress. The bulk modulus is defined as the resistance to volume change and fracture and measures the incompressibility of materials [53]. The V-Ti-Ni alloy also has the highest value of bulk modulus, whereas alloying with Ti and Pd leads to the lowest tolerance against compression compared with other considered alloys and pure V in our calculations. The shear modulus is known as the resistance of material to reversible plastic deformation and is considered as a measure to the hardness of the materials [53]. As shown in *Table 3*, V-Ti-Ni also has the highest shear modulus, which means better performance under external force and imposing shear deformation.

Comparing the value of Poisson's ratio, Pugh's ratio, and Cauchy pressure for pure V and V-Ti-X alloys reveals that all of the considered metals have ductile behavior. Moreover, Poisson's ratio, which provides a measure to define the bonding nature of materials, has a value higher than 0.33, indicating the metallic bonding [59]. Therefore, it could be inferred that the ductility of the considered metals is because of the presence of this kind of bonding. Among the systems, pure V represents more ductility behavior and alloying reduces the ductility nature of the pure V. Furthermore, the highest reduction corresponds to the V-Ti-Ni alloy. The value of hardness increases with alloying that indicates a higher resistance to deformation. V-Ti-Ni has a higher hardness than the other alloys and pure V, being consistent with previous published results, since V-Ti-Ni has the lowest ductility, or higher resistance to deformation.

3. 3. Thermal properties

The thermal and thermodynamic constants provide an understanding about the way of heat conducting and the effect of heat on the materials. Hence, we also calculated these parameters to explore how alloying affects the pure V from this aspect. Sound waves propagate in the matter through vibrations of the particles at their equilibrium interatomic distance [53]. The velocity of the sound waves, as a thermal parameter, depends on the oscillation modes of the particles and provides useful information about thermo-mechanical properties of the material such as thermal conductivity, specific heat, the Debye temperature, etc. [56]. In general, propagation of sound waves in solids takes place through transverse waves and longitudinal waves. Using the Hill's scheme, transverse and longitudinal sound velocities are defined as a function of the elastic constants and are obtained from Eq.(8) [48]:

$$v_l = \left[\frac{B+\frac{4G}{3}}{\rho}\right]^{1/2} ; v_t = \left[\frac{G}{\rho}\right]^{1/2} ; v_m = \left[\frac{1}{3}\left(\frac{2}{v_t^3}+\frac{1}{v_l^3}\right)\right]^{-1/3} \quad (8)$$

Thermal conductivity is a physical nature that indicates the heat transfer capacity of the materials. The minimum value of thermal conductivity is a parameter, measuring the conductivity response of the materials at high temperatures and is calculated from elastic constants [48]. It has a technological importance in many applications for designing and selecting the insulators and adsorbents, the screening of materials and predicting the optimal performance of materials [53]. Using Clarke's model, the minimum thermal conductivity (k_{min}) of materials is described by Eq. (9) [56]:

$$k_{min} = \left(\frac{k_B}{2\pi}\right)\rho_A^{2/3}\left(v_l + v_t + v_m\right) \quad (9)$$

where k_B, and ρ_A are the Boltzmann constant and the atomic density of the structure, respectively. Debye temperature, θ_D is the temperature corresponding to the highest normal vibration mode in the crystal structure. The Debye temperature, in one sense, indicates the strength of the material and its stability and the higher the value, the stronger the interatomic chemical bonding, resulting in high hardness and high melting temperature [53]. Increasing the number of the constituent elements of the structure can also lead to alternation in the Debye temperature which could be interpreted as the variation of the rigidity of the material [60]. It is defined by Eq. (10) [48]:

$$\theta_D = \frac{\hbar}{k_B}\left[\frac{3n}{4\pi}\left(\frac{N_A\rho}{M}\right)\right]^{1/3} v_m \quad (10)$$

where ħ, N_A, ρ, M, and n are Planck's constant, Avogadro number, density, molecular weight, number of atoms in the molecule, respectively. Some other thermal properties can be calculated for pure V and V-based ternary alloys, using the quasi-harmonic Debye model. Hence, the Gibbs non-equilibrium function obtained is expressed as Eq.(11) [61]:

$$G^*(V;P,T) = E(V) + PV + F_{vib}\left[\theta_D(V);T\right] \quad (11)$$

where E(V) is the internal energy per unit cell, P(V) is the constant hydrostatic pressure, T is temperature, and θ(V) is the Debye temperature. F_{vib} is the vibrational Helmholtz free energy and defined as Eq. (12) [62].

$$F_{vib}(\theta_D,T) = nk_BT\left[\frac{9\theta_D}{8T} + 3\ln\left(1-e^{-\frac{\theta_D}{T}}\right) - D\left(\frac{\theta_D}{T}\right)\right] \quad (12)$$

where k_B is the Boltzmann constant, $D(\theta_D/T)$ is the Debye function. Entropy (S) of the crystal is calculated from Eq. (13)[63,64]:

$$S = 3nk_B \ln\left(1 - e^{-\frac{\theta_D}{T}}\right) + 4nk_B D\left(\frac{\theta_D}{T}\right) \quad (13)$$

Grüneisen parameter (γ) describes the effect of the lattice volume change on its vibrational properties. It provides a qualitative relationship between the thermal and mechanical properties of the element as expressed in Eq. (14) [65].

$$\gamma = \frac{V}{C_V}\left(\frac{\partial S}{\partial V}\right)_T = \frac{\alpha B_T V}{C_V} \quad (14)$$

where α, B_T, V, and C_v are the volumetric thermal expansion, isothermal bulk modulus, volume, and constant volume heat capacity, respectively. Mismatches in thermal expansions of compound materials cause thermal stresses at the interface and reduce the adherence to the substrate, hence volumetric thermal expansion is a crucial parameter in many of technological applications [65]. The volumetric thermal expansion coefficient can be obtained from Eq. (15)[66].

$$\alpha = \frac{1}{V}\left(\frac{\partial V}{\partial T}\right)_p = \frac{\gamma C_V}{V B_T} \quad (15)$$

Heat capacity indicates the thermal energy added to the material and the resulting temperature change. The Constant volume (pressure) heat capacity C_v (C_p) is calculated by Eq. (16) and Eq. (17) [67,68].

$$C_V = 12nk_B D\left(\frac{\theta_D}{T}\right) - 9nk_B \frac{\theta_D}{T}\left(\frac{1}{e^{\frac{\theta_D}{T}} - 1}\right) \quad (16)$$

$$C_P = \left(\frac{\partial H}{\partial T}\right)_p = C_V(1 + \gamma\alpha T) \quad (17)$$

All defined thermal parameters including transverse (v_t), longitudinal (v_l) and average (v_m) sound velocities, minimum thermal conductivity (k_{min}), entropy (S), constant volume and pressure heat capacities (C_v and C_p), volumetric thermal expansion (α), enthalpy (H), and Gibbs free energy (G) of pure V and V-Ti-X alloys at 298.15 K are represented in *Table 4*. The predicted value of Debye temperature and Grüneisen parameter for pure V and V-Ti-X alloys in temperature range of 0-1000 K are listed in *Table 5*. In Fig. 2 and Fig. 3, constant pressure heat capacity (C_p) and volumetric thermal expansion (α) of pure V and V-Ti-X alloys are plotted as a function of temperature, respectively.

Table 4 Transverse (v_t), longitudinal (v_l) and average (v_m) sound velocities, minimum thermal conductivity (k_{min}), entropy (S), constant volume and pressure heat capacities (C_v, C_p), volumetric thermal expansion (α), enthalpy (H), and Gibbs free energy (G) of pure V and V-Ti-X alloys at at 298.15 K.

	v_t	v_l	v_m	k_{min}	S	C_v	C_p	A	H	G

		$m.s^{-1}$		$W.mol^{-1}.K^{-1}$	$J.mol^{-1}.K^{-1}$			$10^{-5}.K^{-1}$	$kJ.mol^{-1}.K^{-1}$	
Pure V	2672.346	5964.612	3014.548	1.144	31.249	21.490	21.717	1.904	7.545	0.0860
V-Ti-Al	2701.236	5896.820	3044.135	1.124	31.523	21.386	21.623	1.998	7.583	0.0974
V-Ti-Ni	2927.390	6217.738	3294.687	1.221	31.781	21.422	21.651	1.935	7.568	0.1795
V-Ti-Pd	2596.829	5599.644	2924.796	1.074	32.488	21.414	21.672	2.048	7.570	0.1750

Table 5 Debye temperature (θ_{Debye}) and Grüneisen parameter (γ) of pure V and V-Ti-X alloys at the temperature range of 0–1000 K at 0 GPa.

T (K)	Pure V		V-Ti-Al		V-Ti-Ni		V-Ti-Pd	
	θ_{Debye}/K	Γ	θ_{Debye}/K	γ	θ_{Debye}/K	γ	θ_{Debye}/K	Γ
0.00	376.897	1.857	377.223	1.854	410.374	1.853	360.420	1.963
100	376.774	1.857	377.149	1.854	410.134	1.853	360.197	1.963
200	376.057	1.856	376.780	1.855	408.871	1.854	359.056	1.964
298.15	375.002	1.856	376.304	1.857	407.121	1.857	357.495	1.967
400	373.847	1.857	375.801	1.862	405.154	1.861	355.764	1.972
500	372.653	1.859	375.264	1.869	402.823	1.868	353.718	1.980
600	371.436	1.862	374.694	1.879	399.824	1.878	351.095	1.990
700	370.188	1.867	374.130	1.890	395.932	1.890	347.685	2.002
800	368.902	1.872	373.567	1.904	391.300	1.903	343.612	2.017
900	367.570	1.878	373.010	1.920	386.428	1.919	339.337	2.034
1000	366.214	1.886	372.447	1.938	381.818	1.937	335.278	2.052

Sound wave velocities were also influenced by alloying due to changes in the mechanical characteristics of the metals. As seen in *Table 4*, adding the Ni (Pd) atom increases (decreases) the sound velocities, resulting in an increase (decrease) in thermal conductivity. So, it could be inferred that alloying pure V with Ni increases the heat transfer rate and improves the performance of the structure during the hydrogen related process. Indeed, such processes are mostly exothermic and the released heat is needed to be dispersed in the environment.

Upon alloying and increasing the number of the constituent elements, the interatomic force constants are prone to variation. This leads to a change in vibrational entropy, which can be as large as changes in the configurational entropy and is important for phase stability considerations [69]. The entropy of V-Ti-X alloys have a higher value than the pure V, and V-Ti-Ni has the highest value among these alloys. In contrast, the value of heat capacity for alloys decreases by

alloying the considered elements and the Ni atom addition imposes the highest decrease in both volume and pressure constant heat capacities.

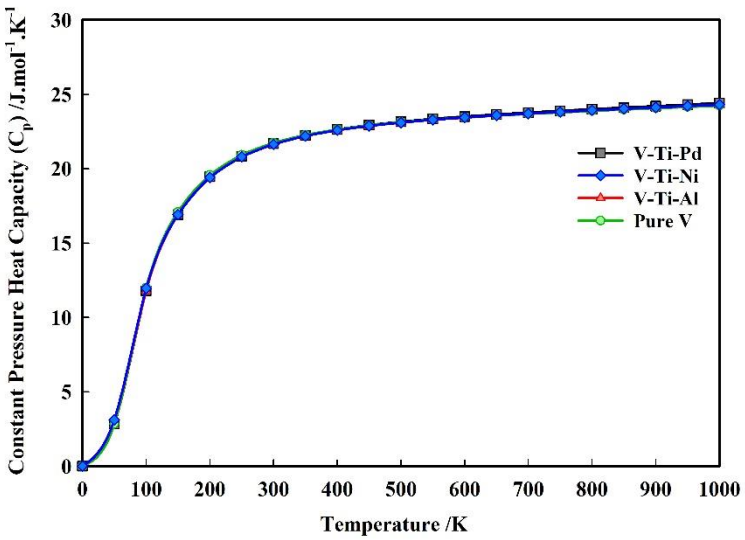

Fig. 2 Evaluated constant pressure heat capacity (C_p) of pure V and V-Ti-X alloys as a function of temperature in vacuum.

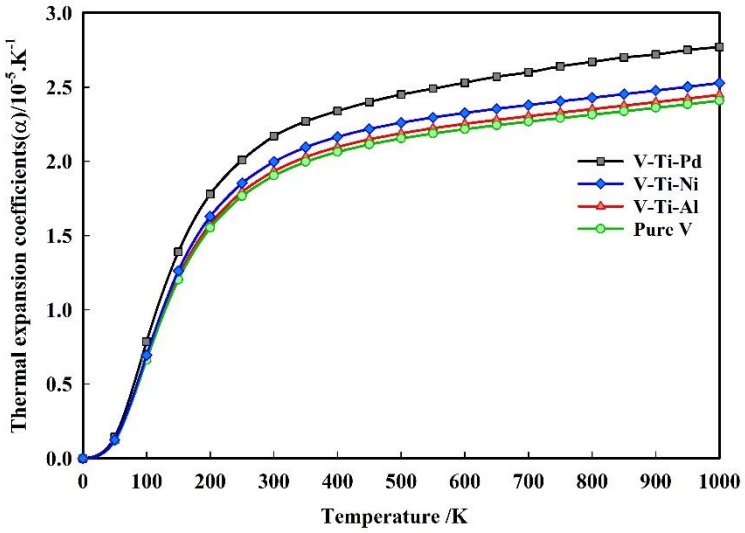

Fig. 3 Evaluated Thermal expansion coefficient (α) of pure V and V-Ti-X alloys as a function of temperature at zero pressure.

As seen in Fig. *2*, the amount of these changes in Cp are marginal compared with the temperature dependence variations and its values are very similar in all the studied materials. Volumetric thermal expansion is also increased by alloying the considered elements and the highest (lowest) change is tailored to the Pd (Ni) atom. Moreover, Fig. *3* represents that the amount of change in α with alloying increases with temperature. Gibbs free energy and enthalpy of alloys are also increased due to the addition of the alloying metals.

As seen in Table 5, the Grüneisen parameter rises as temperature rises, owing to the decreases in volume expansion, bond softening, and increase of the entropy. These are also the origin of the decrease in the Debye temperature. Rate of the changes also grows with the temperature, which is due to the lower resistance of the lattice to the volume change, and also a higher extent of disorder in the system. Alloying imposes variation in these two parameters, so that the V-Ti-Ni has the highest Debye temperature and the lowest Grüneisen parameter among the studied systems. All temperature related justifications are also true for the alloying effect caused by changes in interatomic bonds.

As a conclusion from analyzing the thermal properties, it can be declared that the V-Ti-Ni provides better performance in application tailored to hydrogen-metals systems because of its better heat capacity. It also has a lower temperature induced volume change, which has significance in H-separation, reactor first-wall, and blanket systems. Hence, V-Ti-Ni can be a promising candidate material for the mentioned applications.

3. 4. Electronic properties

Alloying atoms in the structures affect the electrical configuration around the interstitial atoms which leads to variations in chemical interactions between the interstitial atom and its surrounding atoms [33]. This is due to the change in the dissolution of the interstitial atoms. Therefore, the study of changes in the electronic structure of V-Ti-X system is conducive to understanding the H dissolution process and provides important information about the relationship between the physical properties of the material and its bonding nature. To this aim, electronic properties like the total and partial density of states (DOS), and band structure were investigated. The band structures have been calculated by using the corresponding equilibrium lattice parameters along the high-symmetry directions in the first Brillouin zone and in the energy range [-8 to 2 eV] for pure V and the alloys. All calculated band structures have been shown in Fig. 4. The calculated Fermi level energy for pure V, V-Ti-Al, V-Ti-Ni, and V-Ti-Pd are -10.217, -10.375, -10.286, and -10.097 eV, respectively. In all band structures, the energy potential reference is taken at 0 eV and corresponds to the Fermi level. Other energy levels are determined in respect with the Fermi level which is represented by the horizontal dashed line. The spin-up and spin-down bands are depicted by the red and dashed blue lines in the panels. As seen, they completely overlap with each other which is inferred as non-magnetic characteristics of all the structures.

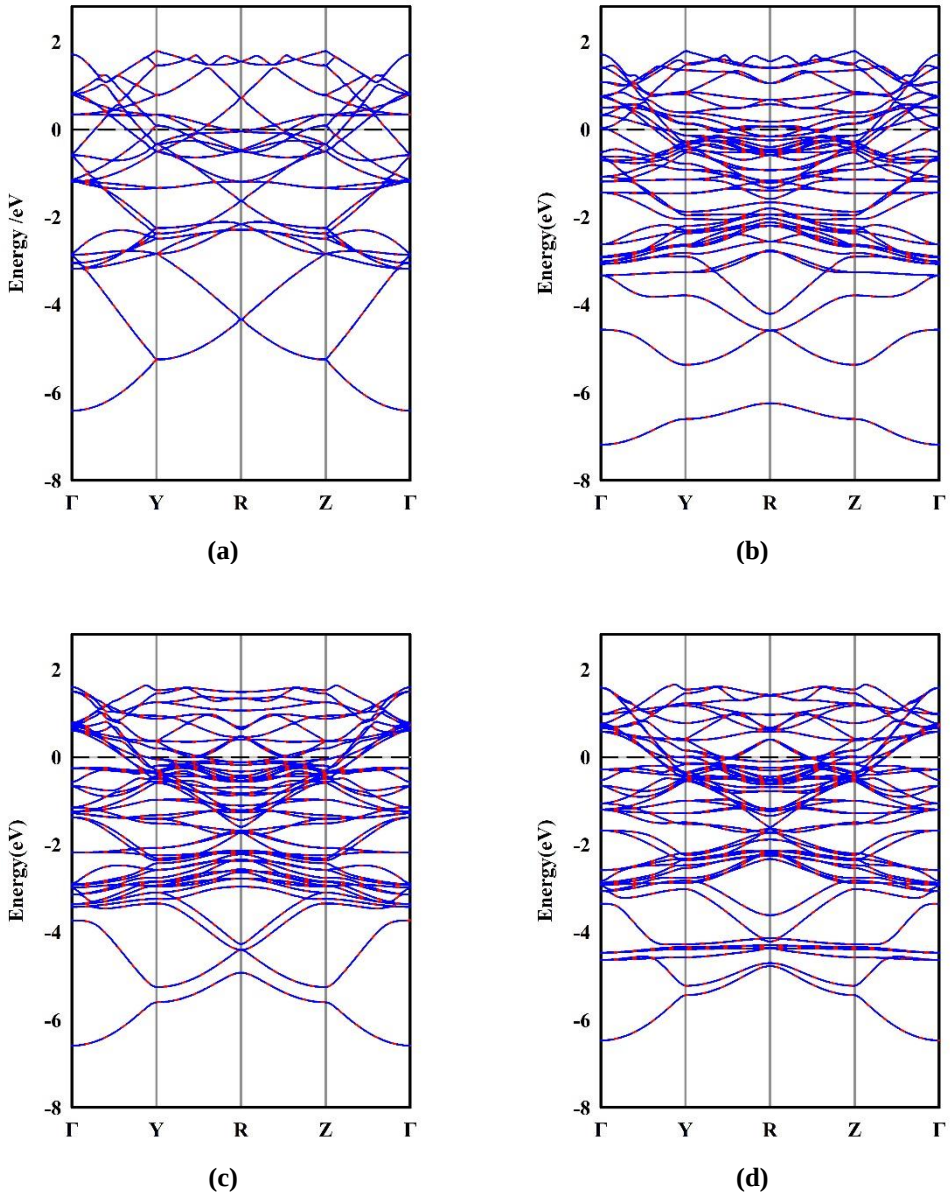

Fig. 4 Evaluated band structure of (a) pure V, (b) V-Ti-Al, (c) V-Ti-Ni, and (d) V-Ti-Pd with the solid red and dashed blue lines for spin up and spin down bands, respectively.

As it was already expected, because of the fully metallic character of the structures, the conduction bands (CB) cross the valence bands (VB), in addition to the crossing of the Fermi energy level for both the spin-up and the spin-down states. Hybridizations between the valence and conduction bands of V-Ti-X alloys are stronger than those of pure V. Hence, there is a larger number of electronic states near the Fermi level and high electronic mobility around the R–symmetry direction. The presence of different transition metals in the alloys leads to the presence of d-orbitals with different energies. The large number of bands in band structures, especially around the Fermi level, is also because of the higher contribution of d-electrons from the TM elements compared to s/p-orbitals. Therefore, it can be inferred that the majority of hybridizations are from the d-d type.

For all the alloys, the band structures have a similar structure and more band crossings take place near the Fermi level along the Γ-Y-R-Z-Γ lines. The energy range of the bands is almost similar with the exception of V-Ti-Al, which has a band near the -7.2eV in the Γ-symmetry point. The stem of all of these electronic states in the band structure can be explored by evaluating the total and the partial densities of states (TDOS and PDOS) of the structures, which also provide a good understanding of the bonding nature of these compounds. In Fig. **5**, the TDOS of all the compounds (pure V and V-Ti-X alloys) are depicted along with the PDOS of all constituent atoms (i.e., V, Ti, Al, Ni, and Pd). The results corresponding to the TDOS of pure V and alloys are consistent with the results of the band structures. TDOS and PDOS plots have the energy spectra from ~-9eV to 4eV and are composed of the valence and conduction bands, overlapping each other. The TDOS values show that all of the compounds have significant electron density contributions at the Fermi level, which mainly stem from the d-orbital of the TMs. The calculated TDOS at the Fermi level for pure V, V-Ti-Al, V-Ti-Ni, and V-Ti-Pd are 28.08, 24.30, 22.17 and 22.31 electrons/eV, respectively. As a preliminary conclusion, it can be inferred that, alloying decreases the density of electrons around the Fermi level and since the state density peak at the Fermi level E_f is not zero, all structures have obvious metallicity.

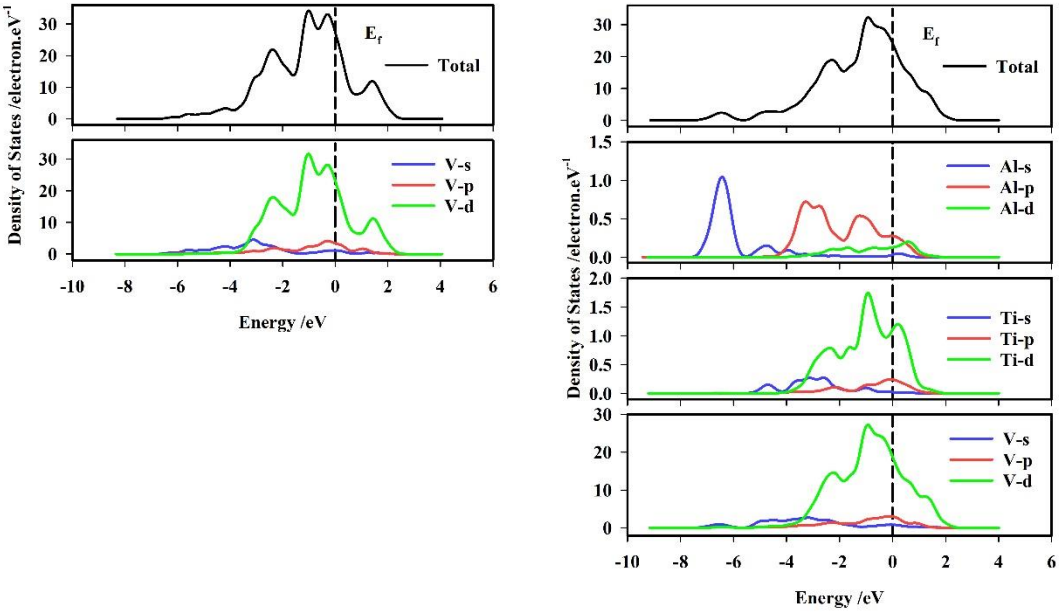

(a) **(b)**

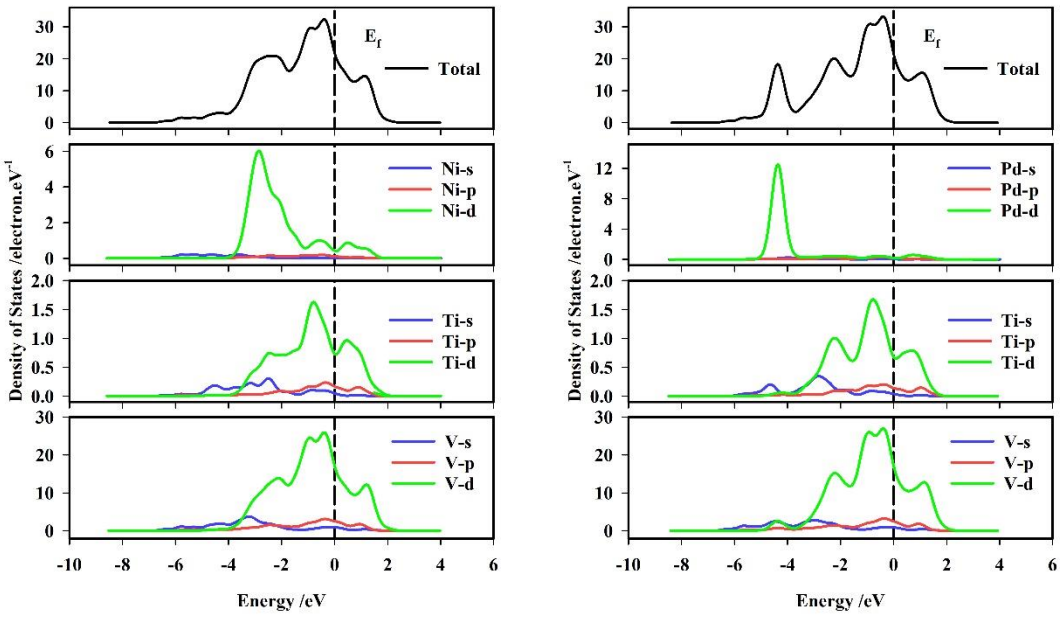

Fig. 5 Evaluated TDOS and PDOS of constituent atoms for (a) pure V, (b) V-Ti-Al, (c) V-Ti-Ni, and (d) V-Ti-Pd.

As seen in Fig. **5**, for pure V, VB and CB are dominated by d-orbitals with a small contribution of s/p electrons in the energy range of -3.8-0 eV for VB and 0-2.2 eV for CB. Out of these ranges, the contribution of d-electrons decreases and its value reaches a lower value than that of s/p-electrons. Alloying pure V with Al, Ni, and Pd leads to the change in the local density of electrons and the distributions over the wider energy ranges. As seen in Fig. **5**-b, the maximum value of total DOS for V-Ti-Al diminished and the energy range was broadened to the lower energy range. Comparing the PDOS of alloys reveals that the s/p/d-orbital electrons of Ti atom have an almost similar contribution in the TDOSs and the minor difference is because of the presence of different adjacent atoms in the compounds. Adding the Al atom, as a post-transition metal with a relatively different electronic configuration, affects its s/p/d-orbital electrons to have an unequal contribution in TDOS compared with the two transition metals (Ni, and Pd). Also, in V-Ti-Al, s/p-orbital electrons have a more contribution than d-orbital electrons, but in the other alloys (V-Ti-Ni, and V-Ti-Pd) d-orbital electrons have a relatively higher contribution than the s/p-orbital electrons. It is worth to be noted that Al, Ni, and Pd mostly have a contribution at the low energy levels in VB.

As it is already seen in the band structure of the alloys, there is higher electron band concentration near the Fermi level compared with pure V. With deep analysis of the PDOS of the alloys, it is observed that different orbitals of several atoms have a contribution in TDOS near the Fermi level, which could be the main reason for this phenomenon.

3.5. Hydrogen dissolution

In this section, dissolution of the H atom in the metals is taken into account, which occurs in interstitial sites (IS). Tetrahedral and octahedral interstitial sites (TISs and OISs) are the two ISs that the H atom most likely occupies. The released energy, due to this occupation, is named solution energy and a more negative value of the energy for an IS indicates a more favorable site to be occupied with the H atom. For investigation of dissolution of hydrogen in V-Ti-X alloys, the solution energy is defined as Eq. (18) [17]:

$$E_{Sol}=E_{Alloy-H}-E_{Alloy}-\frac{1}{2}E_{H_2} \quad (18)$$

where $E_{Alloys\text{-}H}$, E_{Alloy}, and E_{H2} are the total energy of the system when a hydrogen atom is dissolved in V-Ti-X alloys, the energy of V-Ni-M alloys, and the energy of a H_2 molecule in vacuum, respectively. Generally, in the investigation of metal-H systems, the zero-point energy (E_{ZP}) of the H atom must be taken into account which is calculated as Eq. (19) [70]:

$$E_{H,ZP}=\hbar\sum_{i=1}^{3}\frac{\nu_i}{2} \quad (19)$$

where ħ and ν are the the Planck's constant and vibration frequency of a hydrogen atom in each cartesian directions, respectively. The solution energy after E_{ZP} correction can be expressed as Eq. (20) [17]:

$$E_{Sol,ZP}=E_{Sol}+\left[E_{H.Alloy-ZP}-E_{H.H_2-ZP}\right] \quad (20)$$

where $E_{H.Alloy\text{-}ZP}$ and $E_{H.H2\text{-}ZP}$ are the zero point corrected energies of the H atom at the IS of the Alloy and in its molecular form (H_2), respectively. Due to the high symmetry of pure V, there are only two types of IS, including V-surrounded TIS and V-surrounded OIS (V-TIS and V-OIS). In V-Ti-X alloys, ISs have different atoms in their surroundings and this leads to different types of IS, including V-TIS, Ti-TIS, X-TIS, V-OIS, Ti-OIS, and X-OIS (Fig. *6*).

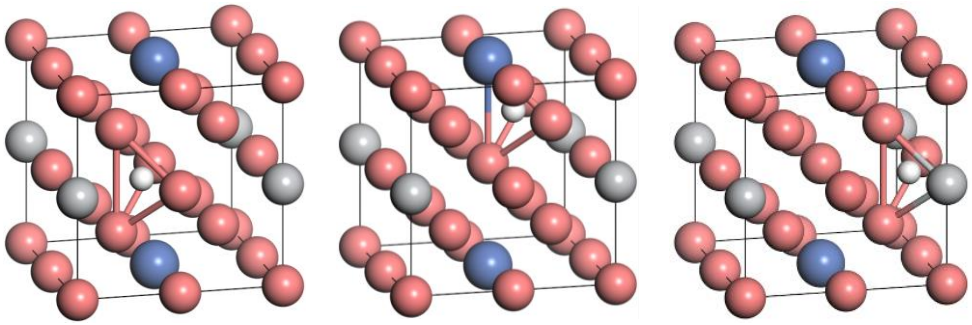

(a) **(b)** **(c)**

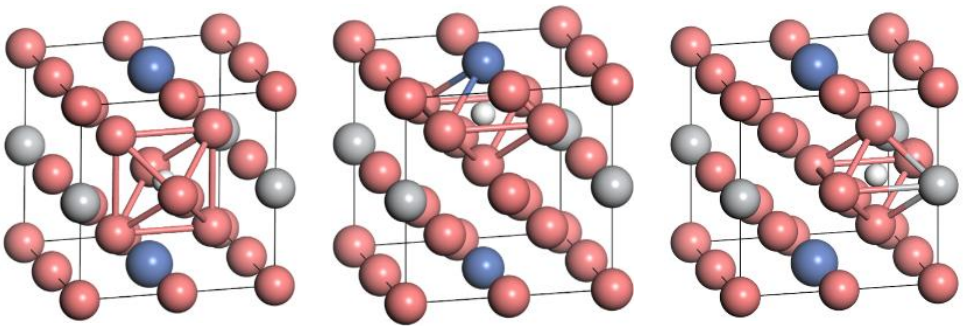

Fig. 6 Different considered interstitial site of the H atom in pure V and V-Ti-X (X=Al, Ni, and Pd), including (a) V-TIS, (b) X-TIS, (c) Ti-TIS, (d) V-OIS, (e) X-TIS, and (f) Ti-OIS. White sphere represents H atom. The other colors have to be mentioned again

The solution energy of the H atom occupied in the ISs of pure V and V-Ti-X alloys are calculated and the results before and after E_{ZP} correction are listed in Table 6. As seen, the solution energies are mostly negative, signaling these H dissolutions in both TIS and OIS are feasible and also stable.

Table 6 solution energies of H atom and its E_{ZP}-corrected value in pure V and V-Ti-X alloys.

	TISs			OISs		
	Site	E_{Sol}/eV	$E_{sol,\,ZP}$/eV	Site	E_{Sol}/eV	$E_{sol,\,ZP}$/eV
Pure V	V-TIS	-0.3592	-0.3371	V-OIS	-0.1742	-0.0596
V-Ti-Al	V-TIS	-0.4188	-0.3925	V-OIS	-0.1962	-0.0827
	Ti-TIS	-0.3449	-0.3216	Ti-OIS	-0.3097	-0.2419
	Al-TIS	-0.4157	-0.3925	Al-OIS	-0.2743	-0.2096
V-Ti-Ni	V-TIS	-0.3274	-0.3097	V-OIS	-0.2280	-0.1183
	Ti-TIS	-0.2912	-0.2731	Ti-OIS	-0.1057	0.0064
	Ni-TIS	-0.3262	-0.3097	Ni-OIS	-0.1695	-0.1137
V-Ti-Pd	V-TIS	-0.4014	-0.3765	V-OIS	-0.1004	0.0142
	Ti-TIS	-0.2770	-0.2581	Ti-OIS	-0.2727	-0.2092
	Pd-TIS	-0.3801	-0.3765	Pd-OIS	-0.2441	-0.1833

In E_{ZP} correction, the vibrational frequencies of the H_2 molecule have great importance. Our calculation for the value of the vibrational frequencies of H_2 is 4394.4 cm^{-1} Which is in good agreement with the previously reported experimental and theoretical values [17,71,72]. The dissolution energies of the H atom occupying TIS before and after E_{ZP} correction for pure V are -0.3592 and -0.3371 eV, respectively, which are more negative than the corresponding value of the H atom occupying OIS (-0.1742, and -0.0596 eV, respectively). This indicates that the TIS is more favorable to be occupied by the H atom in Pure V, which is in agreement with other previous theoretical studies. This is also true for alloys, as V-TISs are more favorable IS for H atom to occupy. It is worth to note that H atom has a different value of frequency in different ISs in the pure V and V-Ti-X alloys, which leads to different E_{ZP}.

The results show that the H atom dissolution more easily takes place in pure V. However, this is more favorable for the separation capacity of metal-hydrogen systems, the resulted HE acts as a

drawback for pure V. Since the solution energy of the H atom is lower in the V-Ti-X alloys, the considered alloying atoms reduce the possibility of hydride formation and improve HE resistance.

Dissolution of H, as an interstitial atom, in the structure of pure V and V-Ti-based alloys affects the characteristics of the structure including electronic, thermal and mechanical properties, etc. The study of changes in electronic properties provides a good understanding of H dissolution and was carried out through the analyzing PDOS of all alloys (Fig. *7*).

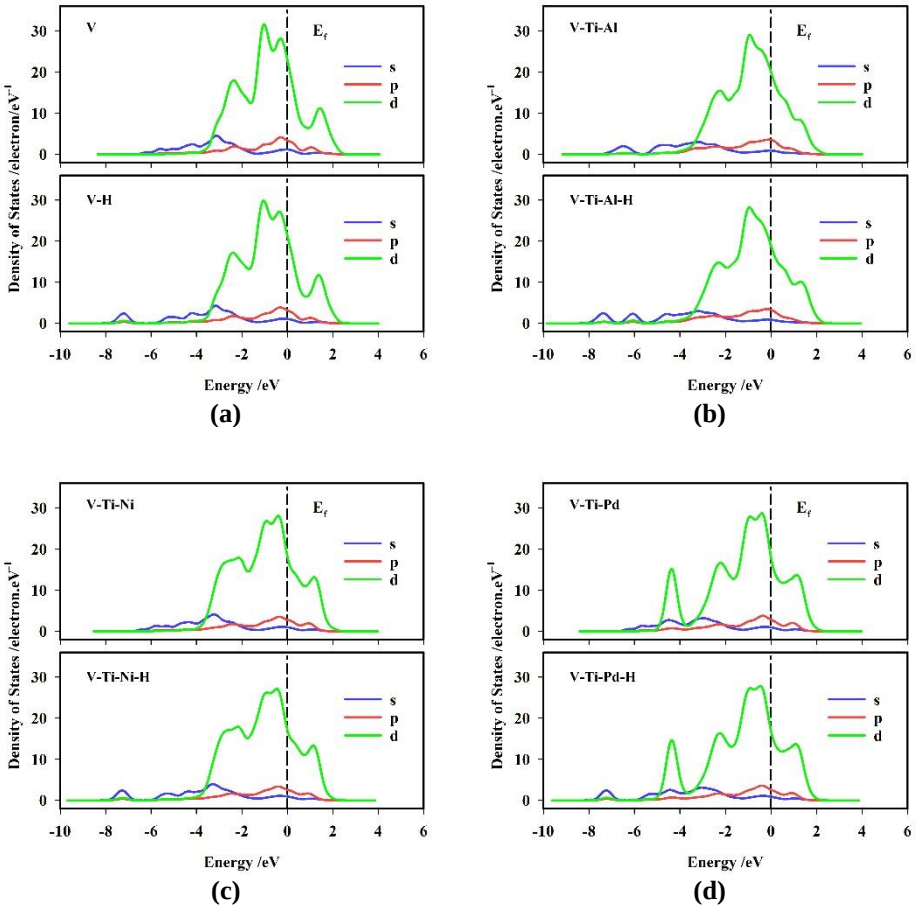

Fig. 7. Evaluated TDOS and PDOS of constituent atoms for (a) pure V, (b) V-Ti-Al, (c) V-Ti-Ni, and (d) V-Ti-Pd.

The results represent that there is a peak at about -7.3 eV in the PDOS of all the alloys. Moreover, the hybridization of the s-orbital electron of the H atom with s/p/d-orbital electrons of the neighboring V and alloying elements forms an H-induced bonding state [16]. This leads to the wider distribution of electrons in lower energies (like -10eV). It is worth noting that in PDOS of V-Ti-Al, there is a peak, which is related to s-orbital of the Al atom, and H-dissolution also imposes a peak in the vicinity of this peak because of its s-orbital electrons. Hence, the hybridization of H-s and Al-s states would impose a repulsion between Al and H and as it is already reported by Q. Hu et al [73], the same phenomenon occurs between H and Al atoms in the V-Ti-Al-H system.

This could be the reason for the lower diffusion barrier energy for the H atom during the diffusion in the V-Ti-Al alloy [17].

Thermal properties are also affected by H dissolution and analyzing the extent of these effects can provide the useful information for their applications. Hence, the effect of H-dissolution on entropy, heat capacities and enthalpy and Gibbs free energy are calculated and the resulted value of these parameters at 298.15 °K are shown in Table 7.

Table 7 The calculated value of entropy (S), constant volume and pressure heat capacities (C_v, C_p), enthalpy (H), and Gibbs free energy (G) of pure V-H and V-Ti-X-H systems at 298.15 °K.

	C_v	C_p	S	H	G
	$J.mol^{-1}.K^{-1}$			$kJ.mol^{-1}.K^{-1}$	
Pure V	21.497	21.724	30.418	9.087	1.826
V-Ti-Al	21.399	21.636	30.606	9.108	1.840
V-Ti-Ni	21.401	21.651	30.897	9.164	1.982
V-Ti-Pd	21.441	21.698	31.775	9.104	1.871

Dissolution of the H atom increases the heat capacities and as seen in Table 7 and Fig. *8*, the V-H and V-Ti-X-H systems have higher values than pure V and the V-Ti-X alloys in the temperature range of 0-1000 K. On the contrary, the entropy of the system decreases upon H-dissolution and the amount of the entropy difference, as seen in Fig. 9, varies at different temperatures. Gibbs free energy and enthalpy of the systems increase and Fig. *10* and Fig. *11* show these enhancements increase with temperature. It is worth to be noted that the V-Ti-Ni alloy is prone to more change in thermal properties upon the dissolution of the H atom.

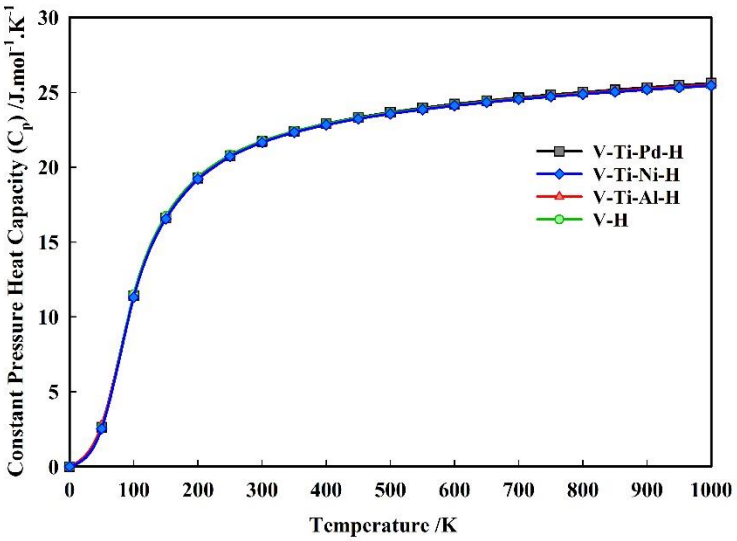

Fig. 8. Evaluated constant pressure heat capacity (C_p) of V-H and V-Ti-X-H systems as a function of temperature at zero pressure.

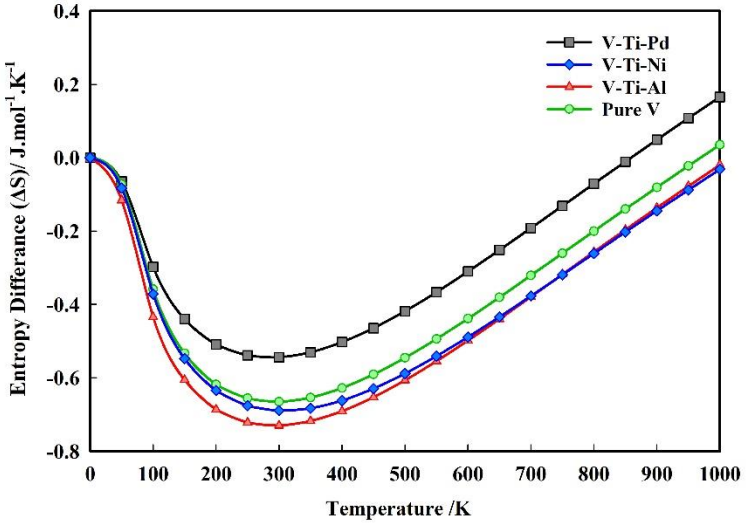

Fig. 9. Entropy difference (Δ*S*) due to dissolution of single H atom in pure V and V-Ti-X alloys as a function of temperature at zero pressure.

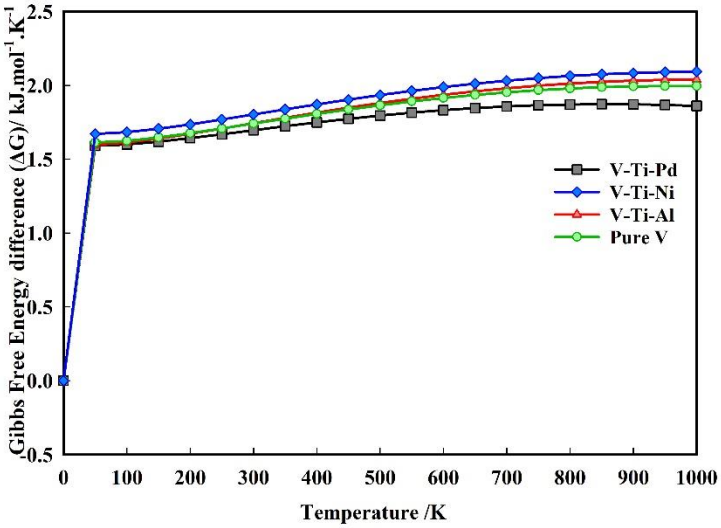

Fig. 10. Gibbs free energy difference (Δ*G*) due to dissolution of single H atom in pure V and V-Ti-X alloys as a function of temperature at zero pressure.

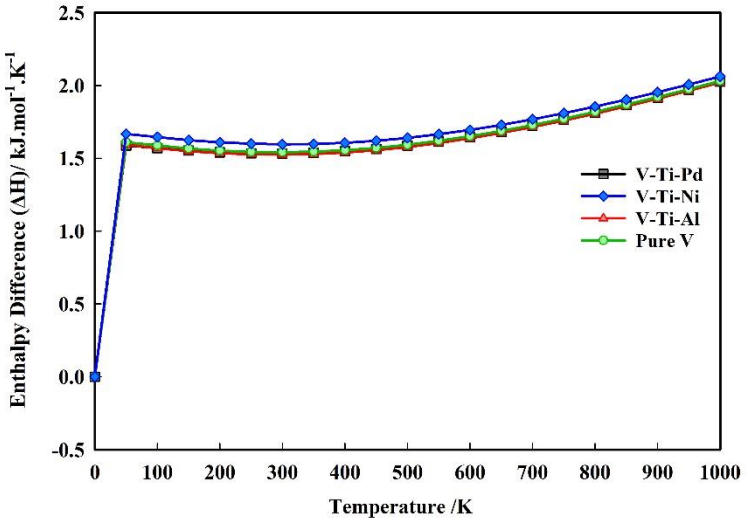

Fig. 11 Enthalpy difference (Δ*H*) due to dissolution of single H atom in pure V and V-Ti-X alloys as a function of temperature at zero pressure.

3.6. H-trapping energy and capacity

HE of metals refers to the stress while the metal is exposed to a high-pressure hydrogen atmosphere, which mostly happens during hydrogen production, absorption, and diffusion in the IS of perfect and defected lattice of metals. Hence, the solubility of H is a characteristic of materials which could be defined by the H solution energy and H-trapping capacity of metals. In section 3.2, dissolution of a single H atom in perfect lattice of pure V and V-Ti-X alloys was taken into account and the solution energies of all TISs and OISs were calculated. Here, the H-trapping capacity of pure V and V-Ti-X alloy for both perfect and defected structures are investigated.

3.6.1. Hydrogen trapping in perfect pure V and V-Ti-X alloys

TISs are the most stable ISs for occupation of the H atom, as concluded in section 3.2. Hence, the H-trapping is performed by the successive dissolution of the H atoms in these ISs and the solution energy is calculated from Eq. (21).

$$E_{H\text{-}trapping} = E_{Alloy\,nH} - E_{Alloy(n-1)H} - \frac{1}{2}E_{H_2} \qquad (21)$$

Fig. *12* shows the solution energy tailored to H-trapping in TISs as a function of the H atom. As shown, pure V has a higher H-trapping capacity than the V-Ti-X alloys and the V-H system is still stable after the 8th H-dissolution. The V-Ti-Al-H system becomes less stable than the other alloys after the 5th H-dissolution and finally the V-Ti-Al-7H turns into an unstable system. The instability of the other alloys occurs after the 8th H-dissolution and they become saturated.

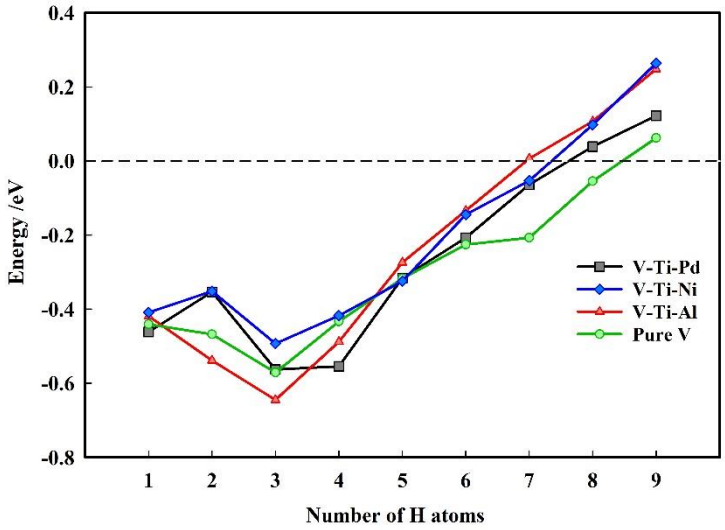

Fig. 12 Solution energy tailored the H-trapping in the TISs as a function of the number of H atoms for pure V and V-Ni-X alloys.

3.6.2. Hydrogen trapping in defected pure V and V-Ti-X alloys

The most basic form of defects in crystalline materials are vacancies, which act as a trap site for impurity atoms (in this case H). Since H-trapping capacity increases due to the emerging of a vacancy in the unit cell, the structure is exposed to more HE. In this section, the dissolution of the H atom in the vicinity of vacancy was taken into account. To do so, a vacancy was substituted for the V atom in pure V and V-Ti-X ternary alloys, and the energy of mono-vacancy structures was calculated using Eq. (22)[17]:

$$E_{f,vac} = [E_{vac} + E_M] - E_p \quad (22)$$

where $E_{f,vac}$, E_p, and E_M are the total energy of the mono-vacancy unit cell, perfect unit cell, and the energy of a single atom. The vacancy formation energies of the V atom in pure V, V-Ti-Al, V-Ti-Ni, and V-Ti-Pd were calculated as 3.252, 2.683, 2.717, and 2.742 eV. So, it could be inferred that alloying increases the resistance against forming a vacancy in the structure and subsequently against HE. Among the considered alloys, V-Ti-Pd alloy is more tolerant of forming a vacancy, which leads to better performance in hydrogen related systems. Interaction of a single vacancy with H atoms was investigated by a successive performing of the dissolution of H atoms in the vicinity of the vacancy and the energy of each step (as trapping energy) was calculated according the Eq. (23) [17,74]:

$$E_{H-Trapping} = E_{V,nH} - E_{V,(n-1)H} - E_{V,1H} - E_V \quad (23)$$

The value of trapping energies as a function of the number of H atoms are depicted in Fig. *13*. As shown, mono-vacancy in pure V has higher H-trapping capacity than the mono-vacancy in V-Ti-

X alloys and it can trap seven H atoms without suffering any instability. At the 7th H-dissolution in mono-vacancy alloys, the system becomes unstable, but this instability occurs at the 8th H-dissolution for pure V. As a conclusion, the investigation of H trapping in IS and vacancy revealed that the V-Ti-Al is more favorable for metal-hydrogen systems.

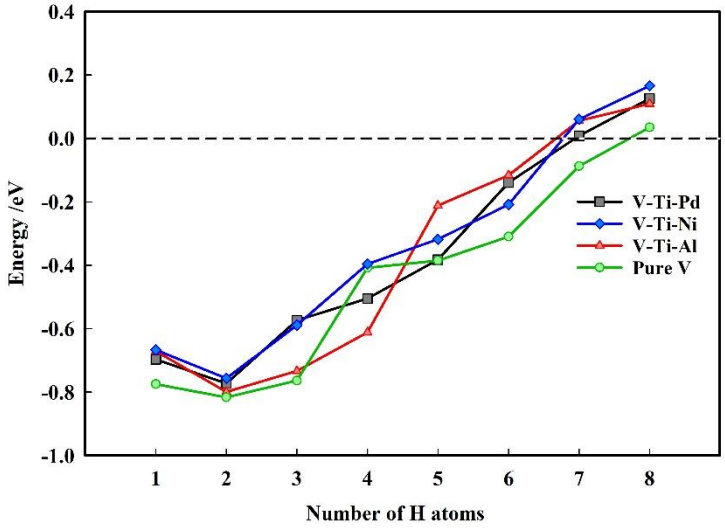

Fig. 13 Dissolution energy trapped H in the vacancy defected pure V and V-Ni-X alloys as a function of the number of H atoms.

3.7. Hydrogen diffusion

Studying diffusion properties provides quite important information on the behavior of atoms (in this case H) in solid structures. The single H atom in vanadium and V-Ni-M alloys hops from one interstitial site to another. In the half of the distance of the entire diffusion path (namely, saddle point position) the energy of the solid reaches its maximum value. The difference between the energy of the initial point and the saddle point is equal the diffusion barrier (E_b). This is the energy required for a single H atom to complete the diffusion and get over moving along a diffusion pathway and is calculated by the NEB method. According to the previous calculations, the H atom is more stable at the TIS. Hence, only the diffusion from one TIS to another adjacent TIS was considered. In Fig. *14*, the diffusion path for a single H atom moving along the [110] direction is shown along with the result of the transition states calculation for V-Ti-Ni alloy with a diffusion barrier energy of 0.1693 eV.

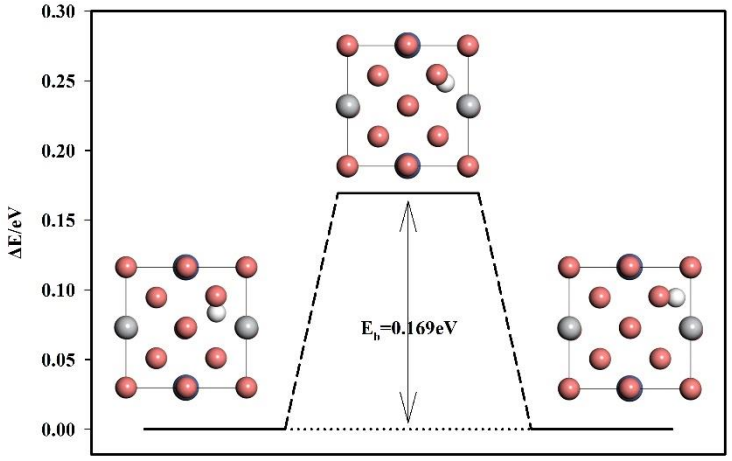

Fig. 14 Diffusion path for single H atom along the [110] direction and barrier energy of single H atom for V-Ti-Ni alloy.

Using the Arrhenius diffusion equation, the hydrogen diffusion coefficient is also obtained from Eq. (24)[75,76]:

$$D = D_0 \exp\left(-\frac{E_b}{k_B T}\right) \quad (24)$$

E_b, k_B and T are the diffusion barrier energy, Boltzmann constant, and absolute temperature, respectively. D_0 is the pre-exponential factor and can be expressed as Eq. (25) for cubic structures of metal [76]:

$$D_0 = \frac{1}{6} n r^2 v, \quad v = \sqrt{\frac{2E_b}{m}} \quad (25)$$

where n, r, and v, m are the numbers of equal diffusion paths, jump length, the vibration frequency, and the mass of the H atom, respectively. In Table 8, the diffusion barrier energy, diffusion distance, diffusion coefficients (at 673 K: the temperature of hydrogen separation in membrane separation application [17]), and the related parameter are provided. In Fig. *15*, the hydrogen diffusion barrier of Pure V and V-Ti-X alloys is depicted in terms of diffusion pathway.

Table 8 Calculated diffusion barrier energy (E_b), diffusion distance (d), vibration frequency (v), pre-exponential factor (D_0), and diffusion coefficient (D) of single H atom in pure V and V-Ti-X alloys at 673 K.

	E_b/eV	d/Å	v/Hz	D_0/cm^2.s^{-1}	D/cm^2.s^{-1}
Pure V	0.1646	1.0609	5.3133×10^{13}	1.9933×10^{-3}	1.1667×10^{-4}
V-Ti-Al	0.1581	1.0548	5.2373×10^{13}	1.9423×10^{-3}	1.2718×10^{-4}
V-Ti-Ni	0.1693	1.0717	5.3348×10^{13}	2.0423×10^{-3}	1.1018×10^{-4}
V-Ti-Pd	0.1807	1.0775	5.4807×10^{13}	2.1211×10^{-3}	9.4103×10^{-5}

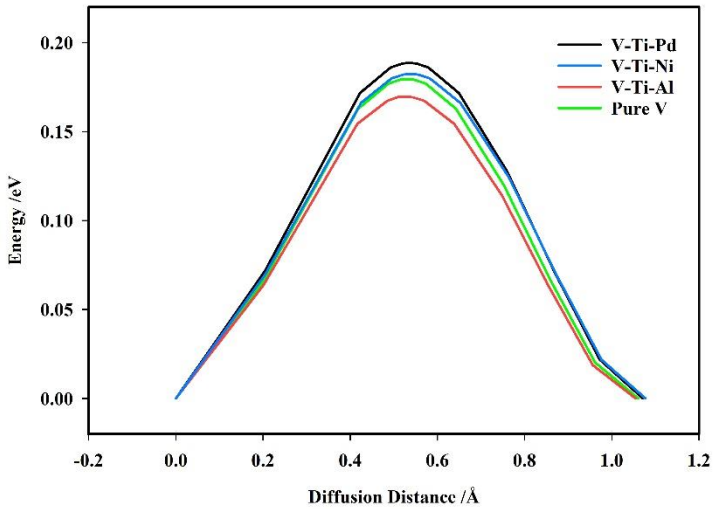

Fig. 15 Diffusion energy curves of single H atom during the diffuse in pure V and V-Ni-X alloys

As seen, the H atom diffusion distance is different for pure V and the alloys and the highest value (1.0775 Å) is for V-Ti-Pd alloy. Starting from the initial position, the energy required for the migration of the H atom gradually increases until the saddle point position. V-Ti-Pd alloy also has the highest diffusion energy barrier (0.1807 eV). So, it can be inferred that the diffusion of the H atom in the V-Ti-Pd takes place in the longest pathway and needs more energy compared with the other solids. On the other hand, the V-Ti-Al has the lowest diffusion barrier energy and the shortest diffusion pathway for the H atom. This could stem from the electronical effect of H-dissolution on the structure and, as inferred in section 3.2, dissolved H imposes repulsion between the Al and H atoms, leading to a lower diffusion barrier energy and a shorter diffusion distance. For hydrogen related applications, V-Ti-Pd alloy provides a favorable candidate from this considered aspect.

In most common hydrogen separation applications, the operation temperature range is between 473-723 K[17]. So, the temperature dependence of the diffusion coefficient (calculated by the Arrhenius diffusion equation) of pure V and V-Ti-X alloys for the temperature range of 100-1000 K was calculated. Using the logarithm function, the exponential relation between temperature and the diffusion coefficient of the alloys was linearly depicted in Fig. *16*.

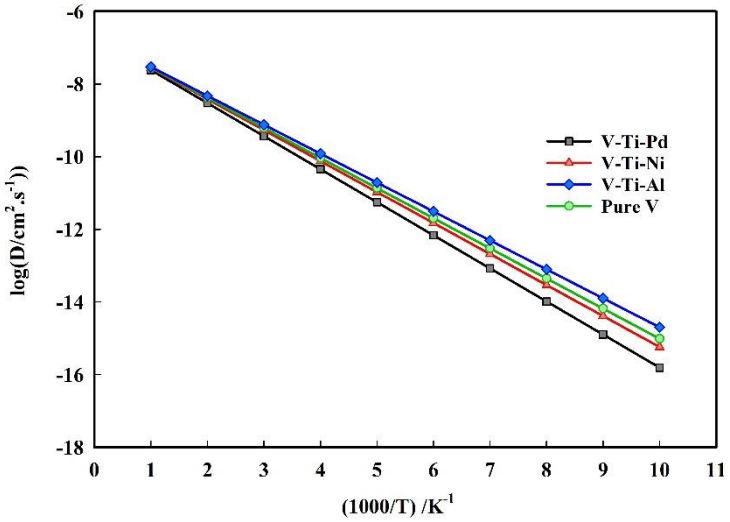

Fig. 16 Logarithmic Arrhenius diagram for diffusion coefficient of single H atom in pure V and V-Ti-X alloys as function of reciprocal temperature.

Among the pure V and considered alloys, the V-Ti-Pd has the highest increase in diffusion coefficient as temperature increases, originating from its highest diffusion barrier. At high temperature, the effect of alloying on the material diminished and this phenomenon can be considered in choosing the material for optimum performance in Hydrogen related applications.

4. Conclusion

The mechanical, thermal, electrical, and hydrogen diffusion properties of pure V and V-Ti-X (X: Al, Ni, and Pd) alloys were investigated using first-principles calculations. According to hydrogen solution energies, H atoms in pure V and the alloys prefer to occupy TISs over OISs. The study of H trapping in perfect and defective structures of pure V and V-Ti-X alloys indicated that mono-vacancy captures 7 and 6 H atoms in pure V and V-Ti-X alloys, respectively, demonstrating the alloys lower H solubility. The V-Ti-Al alloy has the lowest H trapping capacity, according to the results. Furthermore, alloying alters the diffusion barrier energy, affecting the inhibition of hydrogen dissolution and resistance to HE-related problems. In this regard, the V-Ti-Pd alloy provides a better performance. The superior mechanical properties of the V-Ti-Ni alloy indicate that it will be resistant to deformation and have a long service life in hydrogen separation applications. Nonetheless, all alloys are less ductile than pure vanadium, which can be considered a disadvantage of alloying with the metals in question. The V-Ti-Ni alloy has a higher heat capacity than the others, which is important in exothermic processes like hydrogen separation. This research provides a theoretical explanation of the effect of alloying on the hydrogen dissolution behavior of the metals studied. It is expected that the findings are used in experimental investigations for development a novel generation of materials appropriate for hydrogen related processes.

Acknowledgment:

HA and MAB acknowledge the support from Shahid Beheshti University.

Conflict of interest statement:

There is NO conflict of interest.

Reference:

[1] P. Ngene, A. Longo, L. Mooij, W. Bras, B. Dam, Metal-hydrogen systems with an exceptionally large and tunable thermodynamic destabilization, Nat. Commun. 8 (2017) 1–8.

[2] L. Shi, S. Qi, J. Qu, T. Che, C. Yi, B. Yang, Integration of hydrogenation and dehydrogenation based on dibenzyltoluene as liquid organic hydrogen energy carrier, Int. J. Hydrogen Energy. 44 (2019) 5345–5354.

[3] Y. Zhang, P. Wang, Z. Hou, Z. Yuan, Y. Qi, S. Guo, Structure and hydrogen storage characteristics of as-spun Mg-Y-Ni-Cu alloys, J. Mater. Sci. \& Technol. 35 (2019) 1727–1734.

[4] A. Haryanto, S. Fernando, N. Murali, S. Adhikari, Current status of hydrogen production techniques by steam reforming of ethanol: a review, Energy \& Fuels. 19 (2005) 2098–2106.

[5] L. Semidey-Flecha, D.S. Sholl, Combining density functional theory and cluster expansion methods to predict H 2 permeance through Pd-based binary alloy membranes, J. Chem. Phys. 128 (2008) 144701.

[6] M.D. Dolan, Non-Pd BCC alloy membranes for industrial hydrogen separation, J. Memb. Sci. 362 (2010) 12–28.

[7] K. Christmann, F. Chehab, V. Penka, G. Ertl, Surface reconstruction and surface explosion phenomena in the nickel (110)/hydrogen system, Surf. Sci. 152 (1985) 356–366.

[8] L. Qin, C. Jiang, First-principles based modeling of hydrogen permeation through Pd--Cu alloys, Int. J. Hydrogen Energy. 37 (2012) 12760–12764.

[9] S. Adhikari, S. Fernando, Hydrogen membrane separation techniques, Ind. \& Eng. Chem. Res. 45 (2006) 875–881.

[10] P. Kamakoti, D.S. Sholl, Ab initio lattice-gas modeling of interstitial hydrogen diffusion in CuPd alloys, Phys. Rev. B. 71 (2005) 14301.

[11] V. Jayaraman, Y.S. Lin, Synthesis and hydrogen permeation properties of ultrathin palladium-silver alloy membranes, J. Memb. Sci. 104 (1995) 251–262.

[12] T. Maneerung, K. Hidajat, S. Kawi, Ultra-thin (< 1 $μ$m) internally-coated Pd--Ag alloy hollow fiber membrane with superior thermal stability and durability for high temperature H2 separation, J. Memb. Sci. 452 (2014) 127–142.

[13] J.L.C.S. Feitosa, A.G.B. da Cruz, A.C. Souza, F.P. Duda, Stress effects on hydrogen permeation through tubular multilayer membranes: Modeling and simulation, Int. J. Hydrogen Energy. 40 (2015) 17031–17037.

[14] S.-T.B. Lundin, N.S. Patki, T.F. Fuerst, C.A. Wolden, J.D. Way, Inhibition of hydrogen flux in palladium membranes by pressure--induced restructuring of the membrane surface, J. Memb. Sci. 535 (2017) 70–78.

[15] P.G. Sundell, G. Wahnström, Self-trapping and diffusion of hydrogen in Nb and Ta from first principles, Phys. Rev. B. 70 (2004) 224301.

[16] C. Ouyang, Y.-S. Lee, Hydrogen-induced interactions in vanadium from first-principles calculations, Phys. Rev. B. 83 (2011) 45111.

[17] Y. Lu, Y. Wang, Y. Wang, M. Gao, Y. Chen, Z. Chen, First-principles study on the mechanical, thermal properties and hydrogen behavior of ternary V-Ni-M alloys, J. Mater. Sci. \& Technol. 70 (2021) 83–90.

[18] S.K. Dwivedi, M. Vishwakarma, Hydrogen embrittlement in different materials: a review, Int. J. Hydrogen Energy. 43 (2018) 21603–21616.

[19] S. Miraglia, D. Fruchart, N. Skryabina, M. Shelyapina, B. Ouladiaf, E.K. Hlil, P. de Rango, J. Charbonnier, Hydrogen-induced structural transformation in TiV0. 8Cr1. 2 studied by in situ neutron diffraction, J. Alloys Compd. 442 (2007) 49–54.

[20] S. Fasolin, S. Barison, S. Boldrini, A. Ferrario, M. Romano, F. Montagner, E. Miorin, M. Fabrizio, L. Armelao, Hydrogen separation by thin vanadium-based multi-layered membranes, Int. J. Hydrogen Energy. 43 (2018) 3235–3243.

[21] S.N. Paglieri, J.R. Wermer, R.E. Buxbaum, M. V Ciocco, B.H. Howard, B.D. Morreale, Development of membranes for hydrogen separation: Pd coated V--10Pd, Energy Mater. 3 (2008) 169–176.

[22] C. Nishimura, T. Ozaki, M. Komaki, Y. Zhang, Hydrogen permeation and transmission electron microscope observations of V--Al alloys, J. Alloys Compd. 356 (2003) 295–299.

[23] G. Song, M.E. Kellam, D. Liang, M.D. Dolan, Influence of processing conditions on the microstructure and permeability of BCC V--Ni membranes, J. Memb. Sci. 363 (2010) 309–315.

[24] J. Evtimova, E. Drioli, G. De Luca, A density functional theory study of hydrogen occupation in VNiTi alloys used for dense metal membranes, J. Alloys Compd. 665

(2016) 225–230.

[25] M. Okada, T. Kuriiwa, T. Tamura, H. Takamura, A. Kamegawa, Ti--V--Cr bcc alloys with high protium content, J. Alloys Compd. 330 (2002) 511–516.

[26] V.N. Alimov, I. V Bobylev, A.O. Busnyuk, S.N. Kolgatin, S.R. Kuzenov, E.Y. Peredistov, A.I. Livshits, Extraction of ultrapure hydrogen with V-alloy membranes: From laboratory studies to practical applications, Int. J. Hydrogen Energy. 43 (2018) 13318–13327.

[27] A. Rokhmanenkov, Modeling of nonlinear hydrogen diffusion in titanium hydrides TiHx, Int. J. Hydrogen Energy. 42 (2017) 22610–22614.

[28] A. López-Suárez, J. Rickards, R. Trejo-Luna, Mechanical and microstructural changes of Ti and Ti--6Al--4V alloy induced by the absorption and desorption of hydrogen, J. Alloys Compd. 457 (2008) 216–220.

[29] A. Suzuki, H. Yukawa, S. Ijiri, T. Nambu, Y. Matsumoto, Y. Murata, Alloying effects on hydrogen solubility and hydrogen permeability for V-based alloy membranes, Mater. Trans. 56 (2015) 1688–1692.

[30] W.-S. Ko, J.-H. Shim, W.-S. Jung, B.-J. Lee, Computational screening of alloying elements for the development of sustainable V-based hydrogen separation membranes, J. Memb. Sci. 497 (2016) 270–281.

[31] M.D. Dolan, D.M. Viano, M.J. Langley, K.E. Lamb, Tubular vanadium membranes for hydrogen purification, J. Memb. Sci. 549 (2018) 306–311.

[32] K. Sakaki, H. Kim, K. Iwase, E.H. Majzoub, A. Machida, T. Watanuki, Y. Nakamura, Interstitial-atom-induced phase transformation upon hydrogenation in vanadium, J. Alloys Compd. 750 (2018) 33–41.

[33] Y. Lu, M. Gou, R. Bai, Y. Zhang, Z. Chen, First-principles study of hydrogen behavior in vanadium-based binary alloy membranes for hydrogen separation, Int. J. Hydrogen Energy. 42 (2017) 22925–22932.

[34] H. Tschernitschek, L. Borchers, W. Geurtsen, Nonalloyed titanium as a bioinert metal--a review., Quintessence Int. (Berl). 36 (2005).

[35] J. Hua, Y.-L. Liu, H.-S. Li, M.-W. Zhao, X.-D. Liu, Effect of the alloying element titanium on the stability and trapping of hydrogen in pure vanadium: A first-principles study, Int. J. Mod. Phys. B. 28 (2014) 1450207.

[36] K. Ma, E. Lv, D. Zheng, W. Cui, S. Dong, W. Yang, Z. Gao, Y. Zhou, A First-Principles Study on Titanium-Decorated Adsorbent for Hydrogen Storage, Energies. 14 (2021) 6845.

[37] B. Delley, From molecules to solids with the DMol 3 approach, J. Chem. Phys. 113 (2000) 7756–7764.

[38] J.P. Perdew, K. Burke, M. Ernzerhof, Generalized gradient approximation made simple, Phys. Rev. Lett. 77 (1996) 3865.

[39] B. Delley, Hardness conserving semilocal pseudopotentials, Phys. Rev. B. 66 (2002)

155125.

[40] S. Grimme, Semiempirical GGA-type density functional constructed with a long-range dispersion correction, J. Comput. Chem. 27 (2006) 1787–1799.

[41] S. Ehrlich, J. Moellmann, W. Reckien, T. Bredow, S. Grimme, System-dependent dispersion coefficients for the DFT-D3 treatment of adsorption processes on ionic surfaces, ChemPhysChem. 12 (2011) 3414–3420.

[42] S. Grimme, J. Antony, S. Ehrlich, H. Krieg, A consistent and accurate ab initio parametrization of density functional dispersion correction (DFT-D) for the 94 elements H-Pu, J. Chem. Phys. 132 (2010) 154104.

[43] N. Govind, M. Petersen, G. Fitzgerald, D. King-Smith, J. Andzelm, A generalized synchronous transit method for transition state location, Comput. Mater. Sci. 28 (2003) 250–258.

[44] G. Henkelman, G. Jóhannesson, H. Jónsson, Methods for finding saddle points and minimum energy paths, in: Theor. Methods Condens. Phase Chem., Springer, 2002: pp. 269–302.

[45] Y. Kong, Y. Duan, L. Ma, R. Li, Phase stability, elastic anisotropy and electronic structure of cubic MAl2 (M= Mg, Ca, Sr and Ba) Laves phases from first-principles calculations, Mater. Res. Express. 3 (2016) 106505.

[46] D. Hong, W. Zeng, Z. Xin, F.-S. Liu, B. Tang, Q.-J. Liu, First-principles calculations of structural, mechanical and electronic properties of TiNi-X (X= C, Si, Ge, Sn, Pb) alloys, Int. J. Mod. Phys. B. 33 (2019) 1950167.

[47] M.A. Rahman, M.Z. Rahaman, M.A. Rahman, The structural, elastic, electronic and optical properties of MgCu under pressure: A first-principles study, Int. J. Mod. Phys. B. 30 (2016) 1650199.

[48] H. Alipour, A. Hamedani, G. Alahyarizadeh, A. Jahanzadeh, First principle study on the mechanical response of ZrC and ZrN at high-pressure conditions: anisotropy perspective, Mol. Simul. 47 (2021) 1135–1148.

[49] D. Varshney, S. Shriya, Elastic, mechanical and thermodynamic properties at high pressures and temperatures of transition metal monocarbides, Int. J. Refract. Met. Hard Mater. 41 (2013) 375–401.

[50] Y.H. Duan, Y. Sun, M.J. Peng, S.G. Zhou, Anisotropic elastic properties of the Ca--Pb compounds, J. Alloys Compd. 595 (2014) 14–21.

[51] D.I. Bolef, R.E. Smith, J.G. Miller, Elastic properties of vanadium. I. Temperature dependence of the elastic constants and the thermal expansion, Phys. Rev. B. 3 (1971) 4100.

[52] P. Zhang, J. Zhao, B. Wen, Trapping of multiple hydrogen atoms in a vanadium monovacancy: A first-principles study, J. Nucl. Mater. 429 (2012) 216–220.

[53] M. Khanzadeh, G. Alahyarizadeh, A DFT study on pressure dependency of TiC and ZrC

properties: Interconnecting elastic constants, thermodynamic, and mechanical properties, Ceram. Int. 47 (2021) 9990–10005.

[54] R. Tran, Z. Xu, B. Radhakrishnan, D. Winston, W. Sun, K.A. Persson, S.P. Ong, Surface energies of elemental crystals, Sci. Data. 3 (2016) 1–13.

[55] J. Haines, J.M. Leger, G. Bocquillon, Synthesis and design of superhard materials, Annu. Rev. Mater. Res. 31 (2001) 1–23.

[56] L. Chen, X. Zhang, Y. Wang, X. Hao, H. Liu, Microstructure and elastic constants of AlTiVMoNb refractory high-entropy alloy coating on Ti6Al4V by laser cladding, Mater. Res. Express. 6 (2019) 116571.

[57] I.N. Frantsevich, Elastic constants and elastic moduli of metals and insulators, Ref. B. (1982).

[58] Y. Tian, B. Xu, Z. Zhao, Microscopic theory of hardness and design of novel superhard crystals, Int. J. Refract. Met. Hard Mater. 33 (2012) 93–106.

[59] S.N. Tripathi, V. Srivastava, R. Khenata, S.P. Sanyal, Electronic band structure, mechanical and thermodynamic properties of Erbium chalcogenides ErX (X= S, Se and Te): A computational insight, Comput. Condens. Matter. 28 (2021) e00563.

[60] J. Kim, H. Kwon, B. Kim, Y.J. Suh, Finite temperature thermal expansion and elastic properties of (Hf1-xTax) C ultrahigh temperature ceramics, Ceram. Int. 45 (2019) 10805–10809.

[61] A. Otero-de-la-Roza, D. Abbasi-Pérez, V. Luaña, Gibbs2: A new version of the quasiharmonic model code. II. Models for solid-state thermodynamics, features and implementation, Comput. Phys. Commun. 182 (2011) 2232–2248.

[62] D. Ma, B. Grabowski, F. Körmann, J. Neugebauer, D. Raabe, Ab initio thermodynamics of the CoCrFeMnNi high entropy alloy: Importance of entropy contributions beyond the configurational one, Acta Mater. 100 (2015) 90–97.

[63] N. Kumar, S. Kumar, K. Yadav, A. Kumar, P.K. Singh, N. Srivastava, R.P. Singh, Study on thermodynamic, electronic and magnetic properties of RE2Cu2Cd (RE= Dy- Tm) intermetallics: first-principle calculation, Bull. Mater. Sci. 43 (2020).

[64] A. Benmakhlouf, A. Benmakhlouf, O. Allaoui, S. Daoud, Theoretical study of elastic and thermodynamic properties of CuSc intermetallic compound under high pressure, Chinese J. Phys. 57 (2019) 179–188.

[65] F.D. Stacey, J.H. Hodgkinson, Thermodynamics with the Grüneisen parameter: Fundamentals and applications to high pressure physics and geophysics, Phys. Earth Planet. Inter. 286 (2019) 42–68.

[66] G. Grimvall, Thermophysical properties of materials, Elsevier, 1999.

[67] Y.-N. Lin, L.-L. Li, X.-H. Yan, Y.-P. Zhang, D. Zhang, P. Zhang, Elastic and thermodynamic properties of Fe3Ga from first-principles calculations, Solid State Commun. 230 (2016) 43–48.

[68] X. Liu, Q. Feng, B. Tang, J. Zheng, Z. Zheng, W. Zhou, J. Tian, J. Wang, First-principles calculations of mechanical and thermodynamic properties of tetragonal Be 12 Ti, RSC Adv. 9 (2019) 5302–5312.

[69] F. Körmann, Y. Ikeda, B. Grabowski, M.H.F. Sluiter, Phonon broadening in high entropy alloys, Npj Comput. Mater. 3 (2017) 1–9.

[70] P. Kamakoti, D.S. Sholl, A comparison of hydrogen diffusivities in Pd and CuPd alloys using density functional theory, J. Memb. Sci. 225 (2003) 145–154.

[71] K.K. Irikura, Erratum: Experimental Vibrational Zero-Point Energies: Diatomic Molecules [J. Phys. Chem. Ref. Data 36, 389-397 (2007)], J. Phys. Chem. Ref. Data. 38 (2009) 749.

[72] E. Hayward, C.-C. Fu, Interplay between hydrogen and vacancies in $α$-Fe, Phys. Rev. B. 87 (2013) 174103.

[73] Q.M. Hu, D.S. Xu, R. Yang, D. Li, W.T. Wu, First-principles investigation of solute-hydrogen interaction in a $α$-Ti solid solution, Phys. Rev. B. 66 (2002) 64201.

[74] S. Thomas, O. Hildreth, M.A. Zaeem, Unveiling the role of atomic defects on the electronic, mechanical and elemental diffusion properties in CuS, Scr. Mater. 192 (2021) 94–99.

[75] O.O. Bavrina, M.G. Shelyapina, K.A. Klyukin, D. Fruchart, First-principle modeling of hydrogen site solubility and diffusion in disordered Ti--V--Cr alloys, Int. J. Hydrogen Energy. 43 (2018) 17338–17345.

[76] J. Luo, H.-B. Zhou, Y.-L. Liu, L.-J. Gui, S. Jin, Y. Zhang, G.-H. Lu, Dissolution, diffusion and permeation behavior of hydrogen in vanadium: a first-principles investigation, J. Phys. Condens. Matter. 23 (2011) 135501.